Process Zones Observed in a 48 MVA Submerged Arc Furnace Producing Silicomanganese According to the Ore-Based Process

Joalet Dalene Steenkamp, Johan Petrus Gous, Wiebke Grote, Robert Cromarty and Helgard Johan Gous

Abstract Excavation of industrial-scale furnaces allows for the systematic study of reaction sequences by identifying the different reaction zones within the furnace. In 2013, Transalloys excavated a 48 MVA submerged arc furnace that was used for silicomanganese production using the ore-based route. The excavation method was reported elsewhere as was observations made in terms of refractory wear and modes of electrical energy dissipation prior to excavation. The paper presented here, reports on the process reaction zones observed during the excavation and subsequent phase chemical analyses of a number of process samples obtained during the excavation. The zones identified were a loose burden zone, a dry coke-bed zone, a wet coke-bed zone, a hard build-up zone, and an alloy zone. The results are compared to observations made in the excavation of an industrial-scale SAF and a pilot-scale SAF in Norway. The presence of the hard build-up zone below one of the electrodes and absence of a slag zone below all three electrodes are unique features of the SAF excavated at Transalloys.

Keywords Excavation · Dig-out · Silicomanganese · Submerged arc Furnace · Reaction zones

J. D. Steenkamp (✉)
MINTEK, Randburg, South Africa
e-mail: joalets@mintek.co.za

J. P. Gous
Transalloys, Emalahleni, South Africa
e-mail: johang@transalloys.co.za

W. Grote · R. Cromarty · H. J. Gous
University of Pretoria, Pretoria, South Africa
e-mail: wiebke.grote@up.ac.za

R. Cromarty
e-mail: robert.cromarty@up.ac.za

H. J. Gous
e-mail: helgardgous01@gmail.com

B. Davis et al. (eds.), *Extraction 2018*, The Minerals, Metals & Materials Series,
https://doi.org/10.1007/978-3-319-95022-8_50

Introduction

Transalloys, with an annual capacity of 180 000 tonnes is the only producer of silicomanganese (SiMn) in South Africa [1]. SiMn is produced by carbothermic reduction of local manganese ores and quartzite in open submerged arc furnaces (SAFs). Coal and coke are used as reductants. The alloy produced typically contains 65% Mn, 16% Si and less than 2% C [2]. In contrast to the ore based process used by Transalloys a duplex process is commonly used elsewhere in the world. In the duplex process the slag from a high carbon ferromanganese furnace is used as the source of manganese for SiMn production.

The excavation of industrial-scale furnaces allows for the systematic study of reaction sequences by identifying the different reaction zones within the furnace [3–5]. Knowledge of reaction sequences allows for improved understanding of the important characteristics of the raw material and process mechanisms. Understanding of important raw material characteristics allows for the development of rational laboratory–scale techniques suitable for raw material selection [3, 6]. Furthermore, knowledge of the reaction zones could potentially assist with electrode management [4] while knowledge of the process conditions allows for the understanding of refractory wear mechanisms at play [7, 8].

In 2013, a 48 MVA SAF at Transalloys was excavated. Prior to shut down the furnace had been operated at power of 28–30 MW. The excavation method was reported by Gous et al. [9] followed by observations made in terms of refractory wear [8, 10, 11] and modes of electrical energy dissipation prior to excavation [12, 13] by Steenkamp et al. The paper presented here, reports on the process reaction zones observed during the excavation and subsequent phase chemical analysis of some of the process samples.

Methodology

The excavation method reported by Gous et al. [9] can be summarised as follows:

1. Although the intention was to switch out the SAF as close to full load as possible, power restrictions only allowed for the furnace to be operated at 16 MW (as opposed to 30 MW) prior to excavation.
2. The feed charged consisted of 25% coal (50% C), 6% briquettes produced mainly from ore fines screened on site (36% Mn), 18% sintered manganese ore (44% Mn), 35% lumpy manganese ore (38% Mn), 2% alloy fines (66% Mn), and 14% quartzite (99% SiO_2).
3. The tap-hole was plugged half-way through a tapping cycle.
4. The burden was kept as per normal operating conditions with the furnace being filled with raw material mix up to sill level, rather than being burned down as is usually done to speed up the excavation process.

5. Electrodes were suspected to be on length and in good operating condition.
6. To cool down the furnace burden, water was sprayed intermittently from the top for 3 days.
7. The top 1–1.5 m of burden was dug out by hand and mini-front end loader from the top of the furnace.
8. Thereafter, a 4 m by 4 m window was cut in the steel shell between electrodes #1 and #3, and the burden and refractory material were removed using a pecker excavator and sampled by hand. The burden profile and refractory wear profile were determined and recorded by hand.

To study the areas below electrodes #1 and #3, sampling positions were selected and numbered, using green spray paint, as indicated in Fig. 1a and c. In order to sample the burden systematically, the section under investigation was divided into several sub-sections and specific sampling points were identified—see Fig. 1b. At each sampling point, samples were taken from the sill level to the refractory hearth level at 500 mm intervals. Sample numbers indicated column position, e.g. E2XC-, and vertical position within the column. Vertical position numbers started at the top of the bed and increased downward. For example sample E2XC-2 was at a position 1000 mm below the sill level while E2XC-3 was 1500 mm below the sill level. In the order of 200 process samples were taken in this manner.

A burden profile indicating the process zones observed in the furnace was superimposed onto the refractory drawing, based on visual observations made, photographic evidence collected, as well as manual measurements taken during the sampling process. The results were presented in Fig. 2 and the drawing is to scale

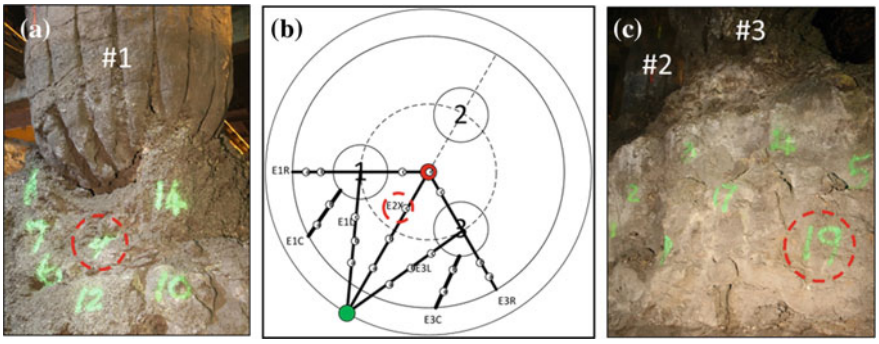

Fig. 1 **a** *Electrode #1* (the tapping electrode) and the coke-bed below, with the *sampling points numbered with spray paint* and the sample reported on elsewhere [13] and referred to in the text indicated with *red dotted lines*. **b** Schematic of SAF in plan view, where the *positions of the sampling columns* of the one-third of the burden excavated between *electrodes #1 and #3* were indicated through a numbering system. The sample column reported on was indicated with *red dotted lines*. **c** *Electrode #3*, with *electrode #2* to the back thereof, with the *sampling points numbered with spray paint* and the sample reported on elsewhere [13] and referred to in the text indicated with *red dotted lines*

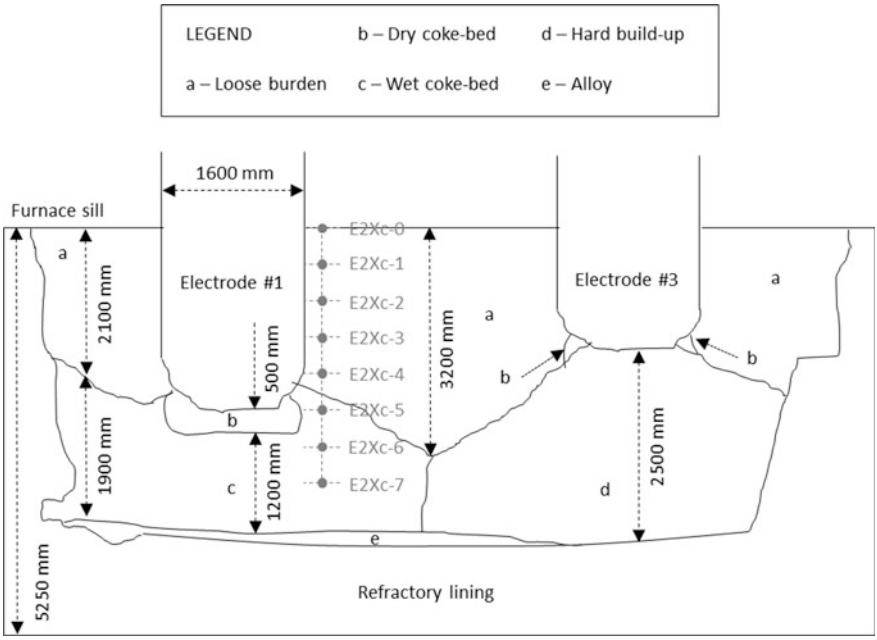

Fig. 2 *Process zones* observed in 48 MVA SAF excavated in 2013 with *typical dimensions* included. Superimposed in grey are the estimated positions of samples E2Xc-0 to E2Xc-7 based on the 500 mm sampling intervals. Note that the sketch is an interpretation of the visual observations made of $\frac{1}{3}$ of the burden presented as $\frac{1}{2}$. At E2Xc the dry cokebed zone will extend further up to allow for E2Xc-4 to be present in the dry coke-bed zone as described below

within the limitations imposed by using manual measurements under excavation conditions.

For practical reasons, the process samples were stored for a number of years before a selection were analysed in 2015 and 2016 at the University of Pretoria (UP) and MINTEK respectively. One column of samples, column E2Xc, was selected for analysis at UP and one sample each below electrode #1 (sample 4) and electrode #3 (sample 19) for analysis at MINTEK. These sampling points were also indicated in Fig. 1a and c. The results from UP are reported here. The results from MINTEK were reported previously [13] and are mentioned here, where applicable.

Quantitative X-ray diffraction (XRD) analysis was applied to determine the bulk phase composition of each sample. A PANalytical X'Pert Pro powder diffractometer in θ–θ configuration with an X'Celerator detector and variable divergence- and fixed receiving slits with Fe filtered Co-Kα radiation ($\lambda = 1.789$ Å) was applied. Phases were identified from the diffractograms using X'Pert Highscore plus

software. The relative phase amounts (weight %) was estimated using the Rietveld method (Autoquan Program) and reported with errors are on the 3 sigma level in Table 2.

Table 1 Photographs of each sample taken from column E2Xc and analysed by QXRD as well as its vertical position with the furnace sill as reference point (photographs provided by Helgard Gous)

Sample Number	Position below sill level (mm)	Sample Number	Position below sill level (mm)
E2Xc-0	0	E2Xc-1	500
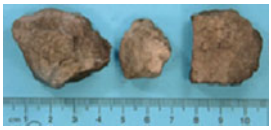			
E2Xc-2	1000	E2Xc-3	1500
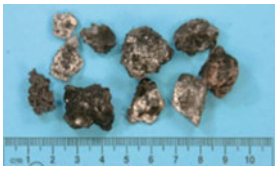			
E2Xc-4	2000	E2Xc-5	2500
			
E2Xc-6	3000	E2Xc-7	3500
			

Results

Furnace Profile

As indicated in Fig. 2, the top part of the burden consisted of loose material. Directly below each electrode, a dry coke-bed was observed. In the case of electrode #3, the dry coke-bed was only observed to the sides of the electrode bottom as opposed to the dry coke-bed observed below the electrode #1. The dry coke-bed formed on top of a wet coke-bed below electrode #1. Below electrode #3, the dry coke-bed formed onto a hard build-up. In the bottom of the furnace, a layer of alloy was observed mainly below electrode #1, in the area between electrodes, and in the tap-hole area. The area below electrode #3 was therefore probably inactive in terms of SiMn production due to the hard build-up. The hard build-up also created problems in terms of electrode management which were discussed elsewhere [13]. Understanding what process conditions would cause the formation of such a hard build-up will be useful in preventing its formation in future but falls outside the scope of this paper.

Phase Composition of Each Zone in Furnace

Table 1 contains a summary of the vertical position of each sample taken from column E2Xc (the furnace sill was the reference point) and photographs of each sample. Table 2 contains a summary of the quantitative XRD analyses of each sample. The results are discussed below in more detail, within the context of the zones identified in Fig. 2. Unfortunately the amorphous content of the samples were not quantified and therefore very little can be said on the amorphous phases i.e. slag, alloy, or carbon contained in the reductant. Furthermore, specific phase chemical analyses, utilising techniques i.e. scanning electron microscopy with energy dispersive spectrometry (SEM-EDS) will be useful in validating the presence of the phases determined by XRD.

Loose Burden Zone

Samples E2Xc-0 to E2Xc-3 were representative of the loose burden zone as its crystalline phase content consisted of phases originally associated with manganese bearing ores from the Kalahari Manganese Field (braunite I, kutnohorite, calcite, and dolomite [14]) and flux (quartzite) as well as phases associated with high temperature dissociation of the ores (manganosite—formed from manganite with an ideal phase composition of MnO(OH)–, johannsenite, and glaucochroite). It is important to note that quartzite was only observed in the loose burden and not in any of the other zones.

Table 2 Quantitative XRD analyses of samples from column E2Xc

Sample number		E2Xc-0		E2Xc-1		E2Xc-2		E2Xc-3		E2Xc-4		E2Xc-5		E2Xc-6		E2Xc-7	
Unit of measurement		wt%	3σ	wt%	3σ	wt%	3σ	wt%	3σ	wt%	3σ	wt%	3σ	wt%	3σ	wt%	3σ
Mineral	Ideal chemical formula																
Braunite I	Mn_7SiO_{12}	9.0	0.6	2.4	0.5	2.2	0.6										
Kutnohorite	$Ca(Mn,Mg,Fe)(CO_3)_2$									2.5	0.5	10.7	1.4				
Calcite	$CaCO_3$	9.7	0.7	8.9	0.9	6.3	1.0										
Dolomite	$CaMg(CO_3)_2$	4.8	0.6			3.4	0.8										
Quartzite	SiO_2	59.7	0.9	70.5	2.0	28.0	1.2	6.2	1.1								
Manganosite	MnO	16.8	0.4	8.0	0.4	34.7	1.1	25.8	1.0	1.6	0.4						
Johannsenite	$CaMnSi_2O_6$			10.3	2.3												
Glaucochroite	$CaMnSiO_4$					24.2	1.6	49.7	2.1								
Andradite I	$Ca_3Fe_2(SiO_4)_3$							2.9	0.6								
Monticellite	$Ca(Mg, Fe)SiO_4$							5.2	1.4								
Spinel	$(Mg, Mn)Al_2O_4$							2.1	0.7					4.4	0.5		
Diopside	$MgCaSi_2O_6$											7.7	0.8	6.1	0.8	10.3	1.7
Bustamite	$CaMnSi_2O_6$									12.4	1.3	56.1	2.1			57.5	4.2
Wollastonite	$CaSiO_3$											8.5	1.4				
Gehlenite	$CaAl(AlSi)O_7$													40.4	1.1		
Magnetite	Fe_3O_4													1.2	0.2		
Wuestite	FeO															2.2	0.5
Cementite	Fe_3C									1.4	0.7						
Manganese carbide	Mn_7C_3							5.6	0.8	2.6	0.7	1.4	0.4	5.5	0.6		
Manganese silicide	Mn_5Si_3									2.8	0.4	6.7	0.5	3.6	0.3	6.2	0.7

(continued)

Table 2 (continued)

Sample number		E2Xc-0		E2Xc-1		E2Xc-2		E2Xc-3		E2Xc-4		E2Xc-5		E2Xc-6		E2Xc-7	
Unit of measurement		wt%	3σ	wt%	3σ	wt%	3σ	wt%	3σ	wt%	3σ	wt%	3σ	wt%	3σ	wt%	3σ
Mineral	Ideal chemical formula																
Manganese carbo-silicide	Mn_5SiC									20.4	1.5	5.3	0.7	6.4	0.5		
Graphite	C									55.6	2.7	2.1	0.7	32.5	1.7	21.8	5.4
Alabandite	MnS							1.8	0.8			1.7	0.3			2.0	0.4
Sylvite	KCl					1.3	0.4	0.8	0.3	0.7	0.2						
Total		**100.0**		**100.1**		**100.1**		**100.1**		**100.0**		**100.2**		**100.1**		**100.0**	

Dry Coke-Bed Zone

Sample E2Xc-4 was an example of the dry coke-bed zone with its crystalline phase content consisting primarily of graphite but also phases associated with the alloy namely manganese carbide, manganese silicide, and manganese carbo-silicide.

Wet Coke-Bed Zone

From the photograph in Table 1, sample E2Xc-5 was an example of the wet coke-bed zone consisting of large reductant particles (black) encapsulated in slag (light-green in colour). The crystalline phase content of the sample consisted mainly of phases associated with slag (bustamite, wollastonite, and diopside [7]), alloy, and graphite. From the phase composition of the crystalline phases present in sample E2Xc-5, E2Xc-6, and E2Xc-7 the coke-bed zone extended further down into the furnace. This is in agreement with the observations recorded in Fig. 2.

Hard Build-Up

A semi-quantitative XRD analysis of the hard build-up conducted previously [13], indicated that the crystalline phases mainly consisted of moissanite (SiC) and portlandite ($Ca(OH)_2$) which was probably a reaction product when calcium carbide (CaC_2) reacted with water used to spray-cool the burden during the excavation. No evidence of either of these phases was found in column E2Xc.

Alloy Zone

None of the samples analysed were representative of the alloy zone.

Discussion

Excavation of a 16 MW SAF in Norway producing SiMn according to the duplex route was reported by Olsen and Tangstad [5]. Zones observed, similar to the ones described in Fig. 2, were the loose burden, the dry coke-bed, the wet coke-bed, and the alloy layer. The location and size of the dry coke-bed was different though: the tips of the electrodes observed by Olsen and Tangstad [5] were immersed in the wet coke-bed with a large, continuous, dry coke-bed forming higher up in the burden. No hard build-up was observed but below each electrode column, zones consisting of slag only were observed. In two pilot-scale experiments reported by Ringdalen and Solheim [15], conducted at 150 and 162 kW respectively, the formation of large dry coke-beds below the electrode tip and wet coke-beds of approximately

equal height, were observed. In this instance, the tips of the electrodes were immersed in the dry coke-beds.

As indicated in Fig. 2, the tips of the electrodes in the 48 MVA SAF were either immersed in a dry coke-bed (electrode #1) or in contact with the hard build-up (electrode #3). It was previously reported [13], through ARCMON measurements, that the slag-to-alloy ratio in the process (and therefor it can be inferred also in the coke-bed) plays a significant role in the mode in which electrical energy is dissipated to the process. It is therefore postulated that more arcing would have occurred in the 48 MVA and 150 kW SAFs than in the 16 MW SAF. It was subsequently reported, again through ARCMON measurements, that the hard build-up resulted in more arcing than the dry coke-bed [13]. It is generally considered that increasing the amount of arcing in an electric furnace will result in increased electrical efficiency, as energy dissipation through arcing is independent of the electrical resistivity of the process material [16, 17], but in SiMn production resistive heating is preferred to ensure stable furnace operation [18].

The size of the coke-bed, as determined by the positions of the electrode tips relative to the alloy layer in the furnace hearth, also plays a role in the stable operations of the SAF. A smaller coke-bed ensures that electrical energy is dissipated to the process in a fashion that ensures all higher oxides of manganese are reduced to MnO when the process temperature reaches 800 °C and the furnace is tapped with ease.

When manganese is present in oxidation states higher than the divalent state at temperatures exceeding 800 °C, it results in increased consumption of both reductant and electricity due to the Boudouard reaction. The reduction of trivalent manganese to divalent manganese in the solid state by CO-gas results in the formation of CO_2. If the local process temperature exceeds 800 °C, the CO_2 will react with carbon according to the highly endo-thermic Boudouard reaction to form CO resulting in the consumption of both carbon and energy. Other reactions that could produce CO_2 are the solid state reduction of iron to the elemental state as well as decomposition of carbonates. It is important to take cognisance of the fact that the production of CO_2 is only a problem in zones where the local process temperature exceeds 800 °C.

Boudouard reaction:

$$C + CO_2 \rightleftharpoons 2CO \tag{1}$$

When a SAF is operated at under-carbon conditions, the process consumes all the carbonaceous reductant charged to the furnace, and a coke-bed is virtually absent [19]. Under-carbon conditions could result in metal that does not meet product specifications and high electrode and carbon-based refractory wear as these become alternative sources of carbon. In a SAF operated under over-carbon conditions, more carbonaceous reductant is charged than required by the process. Over-carbon conditions result in large coke-beds and subsequently in tapping problems or increased power and reductant consumption through the Boudouard reaction, as discussed.

The position of the electrode tips above the alloy layer in the 16 MW SAF were 100, 110, and 50 cm and in the 48 MVA SAF 200, 100, and 250 cm for electrode #1, #2, and #3 respectively. Disregarding the measurement for electrode #3 (as the electrode operated on top of the hard build-up), the coke-bed below electrode #1 could be considered typical of an over-coke condition and that below electrode #2 ideal, in comparison with measurements from the other furnace.

It is expected that the formation of a large coke-bed, and the electrode tip being in contact with a dry coke-bed, with the subsequent observation of increased arcing, go hand-in-hand. Further investigation will be useful.

A question that is often debated in SiMn production is whether or not the alloy is dually saturated in graphite and SiC [8, 20]. If it is the case, then both graphite and SiC will precipitate from the alloy upon cooling. The significant presence of graphite, and absence of SiC, in samples E2Xc-4 to E2Xc-5 is indicative of alloy saturated in graphite rather than SiC, at least for the samples under investigation. In a previous study [13], the semi-quantitative XRD analysis of the hard build-up below electrode 3 (see Fig. 1c) as well as a sample taken from the coke-bed below electrode 1 (see Fig. 1a) indicated that both graphite and SiC were present in both samples. In the sample from the hard build-up, graphite was detected in the range 20–50% by mass and SiC 5–20% by mass. In the sample from the coke-bed, SiC was detected in the range 20–50% by mass and graphite 5–20% by mass. Further investigation of the matter will be useful.

Conclusion

Process zones identified during the excavation of a 48 MVA, industrial-scale SAF applied for the production of SiMn included a loose burden-zone, a dry coke-bed zone, a wet coke-bed zone, a hard build-up zone and an alloy zone. All of these zones, except for the hard build-up zone, were observed previously in an industrial-scale SAF and subsequently in a pilot-scale SAF operated in Norway according to the duplex route. The slag zone, observed in the industrial-scale SAF where SiMn production was based on the duplex route, was not present in the SAF based on the ore-based route.

Work that will be useful in future include:

- Validation of the phases identified by XRD by using scanning electron microscopy with energy dispersive spectrometry (SEM-EDS) .
- Understanding what process conditions will lead to the formation of the hard build-up in the industrial-scale SAF, where SiMn production was based on the ore-based route, and how to prevent it from happening in future.
- Investigation into the correlation between the formation of a large coke-bed, the electrode tip being in contact with a dry coke-bed and observation on arcing, using ARCMON measurements in combination with SAF excavation and post-mortem investigation techniques.

- Further investigation into the presence of graphite and SiC in the SAF excavated to understand the saturation of the alloy in graphite and/or SiC.

Acknowledgements The paper is published with the permission of MINTEK, Transalloys, and the University of Pretoria.

References

1. Gous JP (2018) Optimising slag basicity in the SiMn production process at transalloys. Paper presented at INFACON XV, Cape Town, South Africa, 25–28 February 2018
2. Steenkamp JD, Sutherland JJ, Hayman DA, Muller J (2016) Tap-hole life cycle design criteria: a case study based on silicomanganese production. JOM 68(6):1547–1555
3. Pistorius PC (2002) Reductant selection in ferro-alloy production: the case for the importance of dissolution in the metal. J South Afr Inst Min Metall 102(1):33–36
4. Barcza NA, Koursaris A, See JB, Gericke WA (1979) The "dig out'' of a 75 MVA high-carbon ferromanganese electric smelting furnace. Paper presented at the 37th electric furnace conference, Detroit, Michigan, USA, 4–7 December 1979
5. Olsen SE, Tangstad M (2004) Silicomanganese production–process understanding. Paper presented at INFACON X, Cape Town, South Africa, 1–4 February 2004
6. Tangstad M, Sibony M, Wasbo S, Tronstad R (2001) Kinetics of the prereduction of manganese ores. Paper presented at INFACON IX, Quebec City, Canada, 3–6 June 2001
7. Steenkamp JD, Pistorius PC, Tangstad M (2015) Wear mechanisms of carbon-based refractory materials in silicomanganese tap-holes-Part 1: equilibrium calculations and slag and refractory characterisation. Metall Mater Trans B 46B(2):653–667
8. Steenkamp JD, Pistorius PC, Tangstad M (2015) Chemical wear analysis of a tap-hole on a SiMn production furnace. J South Afr Inst Min Metall 115(3):199–208
9. Gous JP, Zietsman JH, Steenkamp JD, Sutherland JJ (2014) Excavation of a 48 MVA silicomanganese submerged-arc SiMn furnace in South Africa–Part I: methodology and observations. In: Presented at the 5th international symposium on high-temperature metallurgical processing at TMS 2014, San Diego, California, USA, 16–20 February 2014
10. Steenkamp JD (2014) Chemical wear of carbon-based refractory materials in a silicomanganese furnace tap-hole. PhD thesis, University of Pretoria
11. Steenkamp JD, Gous JP, Pistorius PC, Tangstad M, Zietsman JH (2014) Wear analysis of a tap-hole from a SiMn production furnace. Paper presented at the furnace tapping 2014 conference, Muldersdrift, South Africa, 27–29 May 2014
12. Steenkamp JD, Hockaday CJ, Gous JP, Nzima TW (2017) Dissipation of electrical energy in submerged arc furnaces producing silicomanganese and high-carbon ferromanganese. JOM 69(9):1712–1716
13. Steenkamp JD, Hockaday CJ, Gous JP, Clark W, Corfield A (2017) Arcmon for process control in silicomanganese production: a case study. JOM 69(12):2666–2670
14. Chetty D, Gutzmer J (2018) Quantitative mineralogy to address energy consumption in smelting of ores from the Kalahari Manganese Field, South Africa. Paper presented at INFACON XV, Cape Town, South Africa, 25–28 Feb 2018
15. Ringdalen E, Solheim I (2018) Study of SiMn process in a pilot furnace. Paper presented at INFACON XV, Cape Town, South Africa, 25–28 Feb 2018
16. Jones RT (2014) DC arc furnaces–, present, and future. Paper presented at celebrating the megascale: Proceedings of the extraction and processing division, symposium in honour of D. G.C. Robertson at TMS 2014, San Diego, California, 16–20 Feb 2014

17. Jones RT, Erwee MW (2016) Simulation of ferro-alloy smelting in DC arc furnaces using Pyrosim and FactSage. Paper presented at Calphad, Awaji, Japan 29 May–3 June 2016
18. Olsen SE, Tangstad M, Lindstad T (2007) Production of manganese ferroalloys. Tapir Academic Press, Norway
19. Westly J (1974) Resistance and heat distribution in a submerged-arc furnace. Paper presented at INFACON I, Johannesburg, South Africa, 22–26 April 1974
20. Davidsen JE (2011) Formation of silicon carbide in the silicomanganese process. Masters dissertation, Norwegian University of Science and Technology